water

MDPI

Article

Soil Moisture Stochastic Model in *Pinus tabuliformis* Forestland on the Loess Plateau, China

Yi-Fang Chang [1], Hua-Xing Bi [1,2,3,4,*], Qing-Fu Ren [5], Hua-Sen Xu [6], Zhi-Cai Cai [1], Dan Wang [1] and Wen-Chao Liao [7]

1 College of Soil and Water Conservation, Beijing Forestry University, Beijing 100083, China; ella5668@163.com (Y.-F.C.); caizhicai0605@163.com (Z.-C.C.); beilinwangdan@126.com (D.W.)
2 Ji County Forest Ecosystem Research Station, Linfen 042200, China
3 Beijing Collaborative Innovation Center for Eco-Environmental Improvement with Forestry and Fruit Trees, Beijing 102206, China
4 Key Laboratory of State Forestry Administration on Soil and Water Conservation, Beijing Forestry University, Beijing 100083, China
5 State Key Laboratory of Soil Erosion and Dryland Farming on the Loess Plateau, Northwest A&F University, Xianyang 712100, China; wxws.2008@163.com
6 College of Resources and Environmental Sciences, China Agricultural University, Beijing 100193, China; xuhuasen0811@163.com
7 Beijing Water Consulting Co., Ltd., Beijing 100048, China; liaowenchao2009@163.com
* Correspondence: bhx@bjfu.edu.cn; Tel.: +86-10-6233-6756

Academic Editors: Timothy R. Green and Michele Mossa
Received: 25 March 2017; Accepted: 15 May 2017; Published: 18 May 2017

Abstract: As an important restrictive factor of ecological construction on the Loess Plateau, the study of soil moisture dynamics is essential, especially under the impact of climate change on hydrological processes. In this study, the applicability of the Laio soil moisture stochastic model on a typical plantation *Pinus tabuliformis* forestland on the Loess Plateau was studied. On the basis of data concerning soil properties, climate, and plants of the typical forestland during the period 2005–2015 in the Chinese National Ecosystem Research Network (Ji County Station) in Ji County, Shanxi, model results were acquired and compared with observed soil moisture from 2005 to 2015 in the study area. The genetic algorithm method was used to optimize model parameters in the calibration process. In the calibration and validation periods, the relative error between numerical characteristics of simulated and observed soil moisture values was mostly within 10%, and model evaluation index J was close to 1, indicating that the Laio model had good applicability in the study area. When calibrating the model, it was recommended to use soil moisture data with a sampling interval of no more than 10 days so as to reduce the loss of soil moisture fluctuation information. In the study area, the Laio model was strongly sensitive to variations of input parameters, including maximum evapotranspiration rate E_{max}, average rainfall depth α, and average rainfall frequency λ, which should be paid more attention for stable and reliable simulation results. This study offers a method to obtain soil moisture data at ungauged sites. Results from this study provide guidance for Laio model application on the Loess Plateau.

Keywords: soil moisture dynamics; Laio stochastic model; sampling interval; parameter sensitivity analysis; Loess Plateau

1. Introduction

Suffering from severe soil erosion, the Loess Plateau is one of the most fragile ecological environments in the world [1,2]. However, due to a lack of scientific guidance, problems including low survival rate of afforestation and low forest ecological benefits, arose in the implementation process of

vegetation construction projects on the Loess Plateau of China [1,3]. In addition, under the impact of climate change, the characteristics of water supply and demand of ecosystems have been changed [4,5]. Soil moisture, a key variable in hydrological and ecological processes [6,7], is an important restrictive factor of ecological construction on the Loess Plateau. Simulation of soil moisture dynamics has great significance for quantitative research on eco-hydrology, sustainable management of water resources and ecosystems [8], and provides theoretical guidance for ecological construction on the Loess Plateau under the influence of climate change.

Soil moisture can be simulated by remote sensing and hydrologic models. Remote sensing was used to collect near-surface soil moisture over large areas on a routine basis [9]. In order to relate near-surface soil moisture data to the complete soil moisture profile, various assimilation schemes including direct insertion and particle filter were applied to improve soil moisture simulations [9–12]. On the basis of water balance theory, hydrological models can estimate the spatial distribution of soil moisture [13]. Among various hydrological models, the stochastic model can simulate soil moisture at the root zone.

Soil moisture is a continuous stochastic variable and is influenced by uncertain variables in spatial and temporal scales, including climatic factors, soil characteristics, vegetation, topography, and so on. Therefore, soil moisture dynamics exhibit a broad variability and stochastic properties [14–16]. This attribute determines the solution of soil moisture dynamics model should be shown in the form of a probabilistic description [17].

Eagleson introduced rainfall as a random variable into the soil water balance equation and established the stochastic dynamic water balance model in the 1970s [18,19]. On the basis of Eagleson's model, Rodriguez-Iturbe set up a daily soil water balance probability model at a point, and figured out the probability density function (PDF). Laio improved the evapotranspiration calculation method by added two soil moisture thresholds (wilting coefficient and hygroscopic coefficient) into Rodriguez-Iturbe's model, which made the model more accurate when describing the soil moisture dynamics under a water stress environment [20,21]. Ridolfi took topographic factors' impacts on soil water dynamics into consideration [22]. Laio built a simplified probabilistic model of soil moisture temporal dynamics at different soil depths, which depicted soil moisture changes in the vertical direction [23]. Previous soil moisture dynamic stochastic simulation focused on arid regions, however, Rodriguez-Iturbe I et al. [24] first proposed to apply a stochastic model to shallow groundwater-affected ecosystems in humid areas. Laio and Tamea considered the impact of shallow groundwater and capillary flux on soil moisture dynamics in a humid environment, and simulated the dynamics of water level and soil moisture, respectively [25,26].

In China, Huang et al. [27,28] divided the whole year into 16 rainfall periods according to precipitation characteristics on the Loess Plateau, re-calculated the water balance elements and the annual dynamic of soil water content, and used it to replace the simple statistical method of calculating soil moisture in Eagleson's stochastic dynamic water balance model [29], which improved the accuracy and practicability of the model. Subsequently, some Chinese scholars applied the Laio model and the Rodriguez-Iturbe model in different areas, such as mountains [30], hilly areas of basins [31], sandy land [19,21], and irrigated farmland [16,32,33], and they also applied models on different vegetation, including local herbal dominant species, *Artemisia ordosica Krasch.*, *Caragana*, wheat, and corn, to simulate soil moisture dynamics in growing seasons, and discuss the applicability of models in study areas.

With the development of stochastic models, the description of soil water balance components were more detailed [8], and model accuracy and practicability were improved. Nevertheless, there is still some room to improve soil moisture dynamics modelling. The result of a soil moisture dynamic stochastic model is usually shown in the form of a PDF, which is not intuitive when comparing with results of traditional quantitative research. The influencing factors of temporal and spatial distribution patterns of soil moisture should be studied quantitatively in detail, so as to provide support for extrapolating model parameters from the small scale to the large scale.

At present, in the application process of a soil moisture dynamics stochastic model, the study period of data used for model calibration and validation is generally short, ranging from five years to seven years to be exact, and the time resolution of data is low, such as ten days or monthly. Studies based on long-term daily-scale data are scarce, failing to clarify the influence of the data sampling interval on model results. Moreover, the model applicability in forest ecosystems of semiarid regions is still in discussion.

The objectives of this study were (1) to analyze whether model application conditions were satisfied in the study area; (2) to simulate soil moisture on the basis of the Laio model and to evaluate model results by comparing simulated and observed soil moisture values in calibration and validation periods, respectively; (3) to find out the impact of the data sampling interval on model results and provide a theoretical basis for choosing an appropriate data sampling interval; and (4) to examine model sensitivity to variations of input parameters.

2. Theoretical Framework

2.1. Model Descripition

There are many kinds of soil moisture stochastic models; among these models, the Laio model was developed in simulating soil moisture statistical characteristics on the basis of interactions among climate, soil, and plants. Thus, we choose the Laio model to simulate soil moisture in this study.

Based on eco-hydrological process, the Laio model describes the daily water balance within the active soil depth during the growing season. This model investigates influencing mechanisms of soil moisture dynamics on the atmosphere, soil, and vegetation from the perspective of probability and statistics [34], analyzes the impact of interactions among plants, soil, and the environment under different climatic conditions on the soil water balance and plant water conditions, quantitatively evaluates whether the environment is suitable for plants or not, and studies species symbiosis mechanisms [35]. Model results are shown in the form of a PDF.

2.2. Model Principles and Expressions

2.2.1. Assumptions

The Laio model assumes [20]:

1. Rainfall is described as a Poisson process;
2. Soil moisture is uniform in the vertical soil profile within the active soil depth (single soil layer);
3. The influence of the horizontal lateral flow on the soil water balance is ignored;
4. Dynamic interaction between soil moisture within the active soil depth and the phreatic layer is neglected; and
5. Soil water loss is related with soil water content.

2.2.2. Mathematical Expression

According to the water balance principle, soil moisture changes in unit time at a given point equal to the difference of soil moisture input items and output items. The soil moisture balance equation at a given point is expressed as [36]:

$$nZ_r \frac{ds(t)}{dt} = \psi[s(t);t] - \chi[s(t)] \quad (1)$$

where n is the soil porosity, Z_r is the active soil depth (mm), t is the time (d), s is the relative soil moisture ($0 \leq s(t) \leq 1$), $\psi[s(t);t]$ is the rainfall infiltration, and $\chi[s(t)]$ is the soil moisture losses within the active soil depth.

Input items:

$$\psi[s(t);t] = R(t) - I(t) - Q[s(t);t] \tag{2}$$

where $R(t)$ is the rainfall (mm/d). We treated rainfall as a series of point events, and described the occurrence of rainfall as a Poisson process [20]. Each rainfall event was assumed to have a random depth extracted from a given distribution. $I(t)$ is the interception, and $Q[s(t);t]$ is the runoff.

Output items:

$$\chi[s(t)] = E[s(t)] + L[s(t)] \tag{3}$$

where $E[s(t)]$ is the evapotranspiration (mm/d), and $L[s(t)]$ is the deep percolation from the active soil layer (mm/d).

The Laio model introduces two critical soil moisture thresholds: s_h is the soil moisture hygroscopic coefficient and s_w is the wilting coefficient of the soil moisture. These two critical soil moisture thresholds divide the soil evapotranspiration process into evapotranspiration under soil water stress and without water stress conditions [20]. s_h and s_w make the soil moisture content directly related with the soil characteristics and vegetation types when the soil moisture content is low. In the Laio model, leakage is an index function of soil moisture, which makes the soil moisture PDF smoother.

Upon normalization with respect to the active soil depth, the complete form of the losses is summarized as follows:

$$\rho(s) = \frac{\chi(s)}{nZ_r} = \frac{E(s)+L(s)}{nZ_r} = \begin{cases} 0, 0 < s \le s_h, \\ \eta_w \frac{s-s_h}{s_w-s_h}, s_h < s \le s_w, \\ \eta_w + (\eta-\eta_w)\frac{s-s_w}{s^*-s_w}, s_w < s \le s^*, \\ \eta, s^* < s \le s_{fc}, \\ \eta + m\left(e^{\beta(s-s_{fc})} - 1\right), s_{fc} < s \le 1, \end{cases} \tag{4}$$

where $\rho(s)$ stands for the dimensionless loss function to which we will refer hereafter, and:

$$\eta_w = \frac{E_w}{nZ_r} \tag{5}$$

$$\eta = \frac{E_{max}}{nZ_r} \tag{6}$$

$$m = \frac{K_s}{nZ_r\left(e^{\beta(1-s_{fc})} - 1\right)} \tag{7}$$

The stochastic rainfall forcing in Equation (1) makes its solution meaningful only in probabilistic terms. The soil moisture PDF $p(s)$ can be derived from the Chapman-Kolmogorov forward equation for the process under analysis [20]. The PDF is obtained as:

$$p(s) = \begin{cases} \frac{c}{\eta_w}\left(\frac{s-s_h}{s_w-s_h}\right)^{\frac{\lambda'(s_w-s_h)}{\eta_w}-1} e^{-\gamma s}, s_h < s \le s_w, \\ \frac{c}{\eta_w}\left[1+\left(\frac{\eta}{\eta_w}-1\right)\left(\frac{s-s_w}{s^*-s_w}\right)\right]^{\frac{\lambda'(s^*-s_w)}{\eta-\eta_w}-1} e^{-\gamma s}, s_w < s \le s^*, \\ \frac{c}{\eta} e^{-\gamma s+\frac{\lambda'}{\eta}(s-s^*)}\left(\frac{\eta}{\eta_w}\right)^{\lambda'\frac{s^*-s_w}{\eta-\eta_w}}, s^* < s \le s_{fc}, \\ \frac{c}{\eta} e^{-(\beta+\gamma)s+\beta s_{fc}}\left(\frac{\eta e^{\beta s}}{(\eta-m)e^{\beta s_{fc}}+me^{\beta s}}\right)^{\frac{\lambda'}{\beta(\eta-m)}+1} \times \left(\frac{\eta}{\eta_w}\right)^{\lambda'\frac{s^*-s_w}{\eta-\eta_w}} e^{\frac{\lambda'}{\eta}(s_{fc}-s^*)}, s_{fc} < s \le 1 \end{cases} \tag{8}$$

where $p(s)$ is the soil moisture PDF, and c is a constant which can be derived analytically from $\int_{s_0}^{1} p(s)ds = 1$.

The relative soil moisture cumulative distribution function (CDF) $P(s)$ can be obtained by evaluating integrals of $p(s)$:

$$p(s) = \begin{cases} \frac{ca_h}{\eta_w} e^{-\gamma s_h} {c_h}^{-b_h} \{\Gamma(b_h) - \Gamma[b_h, \gamma(s - s_h)]\}, s_h < s \le s_w, \\ P(s_w) + ca_w {c_w}^{-b_w} exp(-\gamma(s_w - \eta_w a_w))[\Gamma(b_w, c_w) - \Gamma(b_w, \gamma(s - s_w) + c_w)], s_w < s \le s^*, \\ P(s^*) + \frac{cb_x}{\eta} \left(\frac{\eta}{\eta_w}\right)^{b_w} \left[exp\left(-\lambda s + \frac{\lambda'}{\eta}(s - s^*)\right) - e^{-\lambda s^*}\right], s^* < s \le s_{fc} \\ P\left(s_{fc}\right) + \frac{c}{m\beta} {x_f}^{-P_f} \left(1 - x_f\right)^{-q_f} \left(\frac{\eta}{\eta_w}\right)^{b_w} exp\left(-\gamma s_{fc} + \frac{\lambda'}{\eta}\left(s_{fc} - s^*\right)\right) \left[B_1 - B\left(x_f e^{-\beta(s - s_{fc})}, p_f, q_f\right)\right], s_{fc} < s \le 1 \end{cases} \quad (9)$$

$$\begin{cases} a_h = s_w - s_h \\ b_h = \frac{\lambda'}{\eta_w} a_h \\ c_h = \gamma a_h \end{cases} \quad (10)$$

$$\begin{cases} a_w = \frac{s^* - s_w}{\eta - \eta_w} \\ b_w = \lambda' a_w \\ c_w = \eta_w \gamma a_w \end{cases} \quad (11)$$

$$b_x = \frac{\eta}{\lambda' - \gamma\eta} \quad (12)$$

$$\begin{cases} x_f = \frac{m - \eta}{m} \\ p_f = 1 + \frac{\gamma}{\beta} \\ q_f = \frac{\lambda'}{\beta(m - \eta)} \end{cases} \quad (13)$$

$$B_1 = B\left(x_f, p_f, q_f\right) \quad (14)$$

$$\begin{cases} \eta = \frac{E_{max}}{nZ_r} \\ \eta_w = \frac{E_w}{nZ_r} \\ m = \frac{K_s}{nZ_r\left[e^{\beta(1 - s_{fc})} - 1\right]} \end{cases} \quad (15)$$

where $\Gamma(:)$ is gamma function, $\Gamma(:,:)$ is the remainder of incomplete gamma function, and $B(:,:,:)$ is the incomplete beta function. A detailed description of the formula's construction can be found in Rodriguez-Iturbe [15] and Laio [20].

2.2.3. Numerical Characteristics of Soil Moisture θ

Relative soil moisture s is used in the calculation process of the Laio model. In this study, expectation $E(\theta)$, standard deviation $\sigma(\theta)$, PDF (probability density function) $p(s)$, and CDF (cumulative density function) $P(s)$ were used to describe numerical characteristics of soil moisture θ in a long-term dynamic process.

$E(\theta)$ is the mean value of θ, which represents the average level of θ during the study period. $\sigma(\theta)$ is the degree of deviation from $E(\theta)$, which shows the fluctuation range of θ during the study period. $p(s)$ reflects the intensity at a given point that can be derived from the Chapman-Kolmogorov forward equation for the process under mathematical analysis [37–39]. θ is the most dense in the vicinity of x_0 which corresponds to the peak of $p(s)$. The area surrounded by $p(s)$ and a specified range is the probability of θ in that range. $P(s)$, which is the integral of $p(s)$, describes the probability distribution of θ, representing the probability in the range of $(-\infty, x)$ when soil moisture is x.

3. Materials and Methods

3.1. Study Area

The study was conducted in the Caijiachuan watershed, Ji County, Shanxi Province, China (35°53′ N–36°21′ N, 110°27′ E–111°07′ E, 1025 m a.s.l.). The area is a typical hill and gully region of the Loess Plateau. It has a temperate continental monsoon climate with rainfall and heat in the same period,

and adequate illumination through the year. The annual average temperature is 10.5 °C (1974–2013) and annual mean rainfall is 523.9 mm (1974–2013). The rainfall is unevenly distributed throughout the year and from June to September contributes to about 70% of the annual precipitation. The annual mean evapotranspiration is 1694.1 mm (1974–2013), which is significantly higher than precipitation during the same period. According to international standards of soil texture classification, the soil texture in the study area is silty loam, with loess parent material and uniform soil properties. Due to the thick soil layer in the Loess Plateau, the buried depth of the groundwater table in the study area is more than 100 m, resulting in a weak hydraulic relationship between the soil water and groundwater. The main afforestation species are Black locust (*Robinia pseudoacacia* L.), Chinese pine (*Pinus tabuliformis*), and Orientalis (*Platycladus orientalis*). The main shrub types are Sea buckthorn (*Hippophae rhamnoides*), Ostryopsis davidiana (*Ostryopsis davidiana*), and Vitex negundo var. (*Cerasus tomentosa*). The main herbaceous species is Dwarf carex (*Carex humilis Leyss*) [40–42].

3.2. Experimental Design

The Laio model was calibrated with soil properties, rainfall, and plant data of the typical artificial vegetation *Pinus tabuliformis* forestland during the period 2005–2011, which contains seven growing seasons (April to October) in the Ji County Forest Ecosystem Research Station and was validated with data of the period 2012–2015, which contains four growing seasons. Model parameters were optimized by a genetic algorithm method. Model results in the calibration and validation periods were compared with observed soil moisture in the same periods. This work is guided on "Observation Methodology for Long-term Forest Ecosystem Research" of National Standards of the People's Republic of China (GB/T 33027-2016).

3.2.1. Experimental Area

Mainly distributed in the middle and lower reaches of the Caijiachuan watershed, *Pinus tabuliformis* forestland constitutes 51.2% of plantation forestland area in the watershed [43]. *Pinus tabuliformis* forestland, which is the typical artificial forestland in the study area, was selected for this study during the period 2005–2015. Trees were planted in 1993 at a spacing of 2 m between trees and 4 m between tree lines (1250 trees·hm^{-2}). The characteristics of trees in June 1995, June 2005, and June 2015 are listed in Table 1. In this area, we designed five plots (4 m in length perpendicular to the tree row, 2 m in width parallel to the tree row). Flat and without obvious salients and sags, each plot included four trees.

Table 1. Basic information of the sample plot.

Date	Average Tree Height (m)	Average Diameter at Breast Height (cm)	Canopy Density
June 1995	2.1	2.2	0.42
June 2005	4.5	6.1	0.63
June 2015	8.5	13.1	0.80

3.2.2. Experimental Period

The growing season (April to October) was chosen as the experimental period because climate and vegetation parameters in a growing season remain constant in time. The model was calibrated with data concerning soil properties, climate, and plants during the period 2005–2011, validated with data during the period 2012–2015, and compared with observed soil moisture in the calibration and validation period, respectively.

3.2.3. Measurement of Soil Moisture θ

A sample point was set in the center of each sample plot. Five sample points were set in total (Figure 1). Soil moisture of each sample point was monitored with an Enviro-SMART Soil Moisture

Profile System (Sentek Sensor Technologies, Stepney, SA, Australia). Soil moisture of the 0–200 cm layer, in 20 cm intervals of the soil profile, was monitored. Determined gravimetrically in each layer, soil moisture was measured every 30 min during the growing seasons of 2005–2015. Real-time monitoring of soil moisture data was maintained with a CR200X Data Logger (Campbell Scientific Incorporation, Logan, UT, USA). The mean soil moisture of 10 layers of five sample points in a day was calculated and used as the daily soil moisture of the experimental forestland. Soil moisture content on the 10th, 20th, and 30th days of each month were extracted and produced a new dataset in which soil moisture was monitored every 10 days. Soil moisture content on the 15th day of each month was selected and formed a new dataset in which soil moisture was monitored every 15 days.

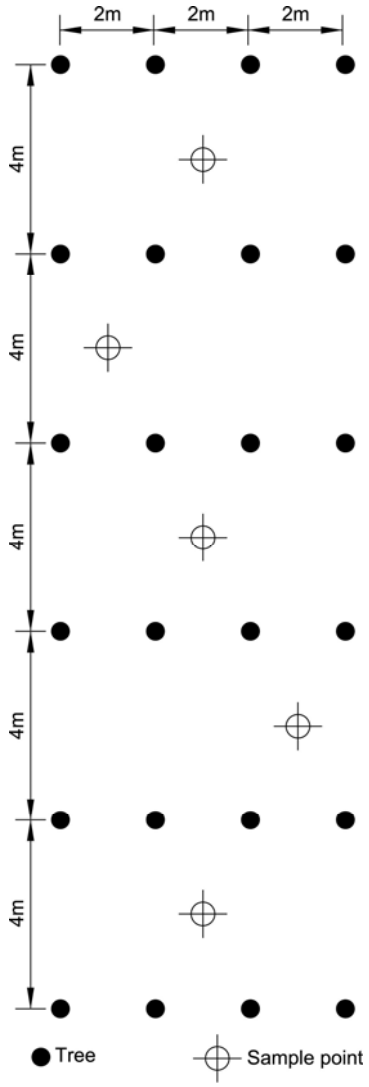

Figure 1. Setting of soil moisture sampling.

3.2.4. Measurement of Rainfall

Rainfall data was collected from a RG3-M Self-recording Rain Gauge (Onset Computer Corporation, Bourne, MA, USA) which was set in an open area near the sample plots, as well as a HOBO Automatic Weather Station (Onset Computer Corporation, Bourne, MA, USA) that was near the sample plots, and the weather station of the Chinese National Ecosystem Research Network (Ji County Station).

3.2.5. Measurements of Soil Porosity n, Field Capacity s_{fc}, Saturated Hydraulic Conductivity K_s

A 100 cm deep soil profile was dug near the sample plots. Undisturbed soil samples were collected using a ring sampler in 20 cm intervals along the soil profile, and used to obtain soil bulk density and field capacity. Three soil samples at each layer were collected as replicates. Soil saturated hydraulic conductivity was determined by the infiltration canister method [44]. The calculation of soil porosity from soil bulk density is expressed as:

$$n = 1 - \frac{W_v}{G_s} \quad (16)$$

where n is the soil porosity, W_v is the soil bulk density (g/cm^3), and G_s is the soil specific gravity (g/cm^3), which is 2.65 g/cm^3 in the Caijiachuan watershed [42].

According to records of Chinese National Ecosystem Research Network (Ji County Station), soil samples were collected every May from 2012 to 2015 for assessing soil physical properties. The average value of soil properties of the 0–100 cm soil layer near *Pinus tabuliformis* sample plots in the validation period (2012–2015) are shown in Table 2. For soil physical properties of the experimental area in the calibration period (2005–2011), refer to Li et al. [45].

Table 2. Soil physical properties of the experimental area in the validation period.

Soil Depth (cm)	Soil Bulk Density (g/cm^3)	Soil Porosity	Field Capacity (%)	Saturated Hydraulic Conductivity (cm/d)
0–20	1.28	0.5181	20.96	145.02
20–40	1.25	0.5299	20.42	52.45
40–60	1.26	0.5252	20.48	5.79
60–80	1.33	0.4990	19.82	9.17
80–100	1.42	0.4645	20.04	10.67

3.2.6. Measurement of Root Biomass

Based on stand survey, three sample trees were selected near sample plots. Assuming the tree trunk as the center, tree roots were almost symmetrically distributed around the tree trunk [46,47]. We idealized tree roots extending as far as 1/2 of distance between trees. Thus, roots that were more than 1/2 of distance between trees were treated as roots of adjacent trees. A 1/4 sample circle method was applied to take samples. In order to measure root biomass accurately, three sample points at the same distance were set at the sample circles whose radiuses were 0.5 m and 1 m (1/2 of distance between trees), respectively, from each sample tree trunk (Figure 2). Root distribution was studied by hierarchical mining methods with a self-made root drill (Root Soil Drill Sampler, CN101482015, 15 July 2009). At each sample point, we excavated and collected tree roots hierarchically in the vertical soil profile, which was divided into five soil layers (0–20 cm, 20–40 cm, 40–60 cm, 60–80 cm, 80–100 cm). After crushing and sieving soil, picking roots from the soil, and cleaning root surfaces, the root diameter d was measured with a vernier caliper. According to standards in a previous studies [48], roots were classified into two groups: coarse roots ($d \geq 2$ mm) and fine roots ($0 < d < 2$ mm). All of the roots were dried at 75 °C in an oven, and weighed, respectively. We set 18 sample points around three sample trees (each sample tree had six sample points) in August 2015. The root biomass of each soil layer was the average of root biomass of all the sample points at the same layer.

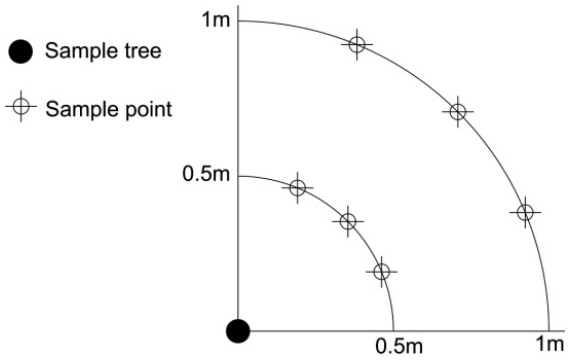

Figure 2. Setting of roots sampling.

3.2.7. Data Resource of Model Parameters

Except for measurement, some model parameters were collected from the Chinese Ecosystem Observation and Research Dataset—forest ecosystems volume (Ji County Station, Shanxi Province, 1978–2006) [43] and related literatures in the same study area (Table 3).

Table 3. Data resource of some model parameters.

Parameters	Data Resource
Soil porosity distribution parameter β	Laio et al. [20]
Hygroscopic coefficient s_h	Li [45]
Wilting coefficient s_w	Li [45]
Soil evaporation at wilting point E_w (cm)	Laio et al. [20]
Canopy interception threshold Δ (cm)	Ciren [49]
Maximum evapotranspiration rate E_{max} (cm)	Pan [50]

Generally, plants are not subject to water stress when soil moisture is higher than 80% of the field capacity [51]. Thus, we selected 80% of the field capacity as the critical soil moisture below which plants undergo water stress s^*.

3.3. Data Analysis

3.3.1. Calculation of Relative Soil Moisture s

Based on the soil moisture of different soil layers in the sample plots monitored by the Enviro-SMART system, soil moisture θ in the active soil layer was obtained by a weighted average method. θ should be standardized and converted to relative soil moisture s because the input item of the Laio model is s. The calculation of s is expressed as:

$$s(t) = \frac{\theta(t)}{n} \tag{17}$$

where $s(t)$ is the relative soil moisture at t time, $\theta(t)$ is the volumetric soil moisture content at t time (%), and n is the soil porosity.

3.3.2. Calculation of Average Rainfall Depth α and Average Rainfall Frequency λ

According to Chinese national classification standards of rainfall levels, the average rainfall depth α of the Laio model was calculated from rainfall amount of different rainfall levels by the weighted average method [16].

$$\alpha = \sum_{i=1}^{k} (\alpha_i \times f_{\alpha i}) \tag{18}$$

where α is the average rainfall depth (mm), α_i is the average rainfall amount at level i (mm), $f_{\alpha i}$ is the relative frequency at level i, and k is the number of rainfall levels.

Average rainfall frequency λ of the Laio model was calculated from relative frequency of different rainfall intensity levels by the weighted average method [16].

$$\lambda = \frac{1}{\sum_{i=1}^{p}(\tau_i \times f_{\tau i})} \tag{19}$$

where λ is the average rainfall frequency, τ_i is the number of interval days of adjacent rainfall events at level i, $f_{\tau i}$ is the relative frequency of interval days of adjacent rainfall events at level i, and p is the number of interval days levels.

3.3.3. Calculation of Active Soil Depth Z_r

In the Laio model, the active soil depth Z_r was set as the distribution range of more than 95% of root biomass [20]. In this study, root biomass density was used to compare root biomass in different soil depths. Root biomass density is an important indicator of the underground growth and the most direct indication of root growth [51]. The calculation of root biomass density is expressed as:

$$RD_w = \frac{W_d}{V_s} \tag{20}$$

where RD_w is the root biomass density (g/m^3), W_d is the root dry biomass (g), and V_s is the soil volume (m^3). Soil volume was calculated by $V_s = \pi R^2 h$, where R is the root drill radius, which was 0.05 m in this study; h is the root sample depth, which was 0.2 m in this study [52].

3.3.4. Parameter Calibration

Relative soil moisture s in 2005–2011 was used to calibrate the Laio model and s in 2012–2015 was used to validate the model.

According to reference literature and experimental data, some parameters of the Laio model fluctuate in certain ranges. Thus, a genetic algorithm method was used to optimize six parameters, including β, s_h, s_w, s^*, s_{fc}, and E_{max} in the Laio model. The ranges of parameters were given as follows, respectively: β [12, 15], s_h [0.01, 0.20], s_w [0.10, 0.25], s^* [0.30, 0.60], s_{fc} [0.30, 0.70], and E_{max} [0.10, 0.90]. In the process of parameter calibration, the population number was 50, the crossover rate was 0.8, the mutation rate was 0.001, the iteration number was the calculation times when the fitness of all of the individual populations was stable within the range of ± 0.0001, and the goodness of fit χ^2 was the fitness.

$$f\left(\chi^2 \middle| \beta, s_h, s_w, s^*, s_{fc}, E_{max}\right) = C_m - \chi^2 \tag{21}$$

$$\chi^2 = \sum_{i=1}^{b} \frac{\left(N_{ob}^i - NP_{mb}^i\right)^2}{NP_{mb}^i} \tag{22}$$

where $f\left(\chi^2 \middle| \beta, s_h, s_w, s^*, s_{fc}, E_{max}\right)$ is the fitness; C_m is a constant, which was 10,000.0 in this study; χ^2 is the chi-square value; b is the total group number of the soil water content; $N^i{}_{ob}$ is the number of observed values in the interval of i; N is the number of the whole observed values; $P^i{}_{mb}$ is the simulation probability in the interval of i.

Soil moisture values whose frequency was greater than five were automatically divided into a group by MATLAB R2014a (The Math Works, Natick, MA, USA). The number of observations $N^i{}_{ob}$ at interval i was obtained according to the input soil moisture and the soil porosity. The chi-square test was used to examine whether there was a significant difference between the observed and simulated values. The null hypothesis of the chi-square test of the observed soil moisture comes from the overall distribution of the simulation results $P(s)$. The confidence level is 0.90, n_n is the degree of freedom, n_n

$= b - 1$, and the critical value of the chi-square distribution is ${\chi^2}_{0.10}\ (n_n)$. If $\chi^2 < {\chi^2}_{0.10}\ (n_n)$, then the simulated values passed the chi-square test. The smaller the chi-square value was, the better the simulation results.

3.3.5. Model Evaluation

The coherence degree of observed and the simulated soil moisture in the calibration and validation periods were evaluated by relative error *RE* and consistency index *J*:

$$RE = \frac{|\theta_o - \theta_m|}{\theta_m} \tag{23}$$

where θ_o is the observed soil moisture; θ_m is the simulated soil moisture.

$$J = 1 - \frac{\sum_{i=1}^{b} \left(f_{o\theta}^{i} - f_{m\theta}^{i}\right)^2}{\sum_{i=1}^{b} \left(f_{o\theta}^{i} - \overline{f_{o\theta}}\right)^2} \tag{24}$$

where $f_{o\theta}^{i}$ is the frequency of the observed soil moisture in the interval of i; $f_{m\theta}^{i}$ is the frequency of the simulated soil moisture in the interval of i; $\overline{f_{o\theta}}$ is the average of the observed soil moisture frequency. The value of the consistency index J ranges from negative infinity to 1. If J is close to 1, the model credibility is high; if J is close to 0, the simulation results are close to the average level of the observed values, indicating that the overall simulation results are credible, but the simulation error in the process is large; if J is far less than 0, the model is not credible.

3.3.6. Parameter Sensitivity Analysis

The fluctuation of the model parameters greatly influenced the stability and reliability of the model. There were 13 parameters concerning soil, plants, and rainfall in the Laio model and some parameters had a large range of fluctuation. Thus, it was necessary to analyze parameter sensitivity.

In this study, under the condition that we made one parameter increase or decrease 10% of the optimum value and other parameters remained the same, the influence of parameter variation on the peak value and its position, the 90% confidence interval of $p(s)$ was analyzed, and the degree of parameter sensitivity was evaluated.

3.3.7. Statistical Analyses

Numerical characteristics of soil moisture θ, including mean value, standard deviation, quartile values, and relative error were calculated by SPSS 20.0 (IBM, New York, NY, USA). Six parameters, including β, s_h, s_w, s^*, s_{fc}, and E_{max} were optimized by a genetic algorithm method using MATLAB R2014a (The Math Works, Natick, MA, USA) and the Laio model was also run by MATLAB R2014a. Model results were shown in pictures drawn by Origin 9.1 (Origin Lab, Northampton, MA, USA).

4. Results

4.1. Analysis of the Model Application Conditions in the Study Area

4.1.1. Analysis of Rainfall Characteristics

The Poisson process is a basic independent incremental process of the occurrence number of random events. Precipitation can be regarded as a random event. The occurrence of precipitation in the study area accords with the form of the Poisson process, because:

1. It assumes no precipitation event occurred at the initial time;
2. The number of precipitation events occurring in any non-overlapping time intervals is independent of each other. That is, the number of precipitation events occurring in each day, each month, and each year does not influence each other;
3. In the time interval of $[t, t + h]$, the number of rainfall events is only related with the time interval h, and independent of the time origin point t; and
4. Within a time interval h which tends toward zero, the probability that an event occurred more than twice is quite small. That is, the probability of the occurrence of two or more precipitation events in a short time is very small.

To sum up, the rainfall in the study area was consistent with the Laio model hypothesis that the occurrence of precipitation in the study area is in the form of the Poisson process.

According to the Chinese national classification standard of rainfall levels, rainfall in 2005–2015 were classified and analyzed. The rainfall frequency of various rainfall levels are depicted in Table 4. Light rain and moderate rain are the main types of rainfall in the study area. Calculated by weighted average method, the average rainfall depth in the growing season α was 7.059 mm in the calibration period (2005–2011), and 6.639 mm in the validation period (2012–2015).

Table 4. Rainfall frequency of all intensity levels in 2005–2015 growing seasons.

	Rainfall Levels						**Total**
	Light Rain	**Moderate Rain**	**Heavy Rain**	**Rainstorm**	**Heavy Rainstorm**	**Torrential Rain**	
Rainfall amount (mm)	(0, 10)	[10, 25)	[25, 50)	[50, 100)	[100, 250)	[250, ∞)	
Rainfall events	582	106	34	10	1	0	733
Relative frequency	0.7940	0.1446	0.0464	0.0136	0.0014	0	1.0000

According to the frequency statistics of rainfall interval days, the interval period of two adjacent precipitation events mainly ranged from 1 to 8 days, and its cumulative frequency was 0.8688. The long interval period of two adjacent precipitation events mainly ranged from 15 to 19 days. In the calibration period (2005–2011), the average rainfall frequency λ of the Laio model was 0.3224, while in the validation period (2012–2015) λ was 0.3205.

4.1.2. Characteristics of Active Soil Depth Z_r

The Laio model assumes the soil moisture was homogeneous in the vertical direction of the active soil layer. The active soil depth Z_r depends on vertical root distribution and was identified as a distribution range of more than 95% of root biomass [20]. Studies including Wang et al. [53], Lei Yang et al. [54], Jun Li et al. [55], Niu and Zhao [56] found that soil moisture was homogeneous in the root layer, and it was obviously different from the soil moisture below the root layer on the Loess Plateau, which satisfied the Laio model assumption.

Fine roots of trees affect the utilization of soil moisture and nutrients by the forest. According to vertical distribution of root biomass density (Table 5), root biomass density of *Pinus tabuliformis* forestland concentrated in the soil layer of 0–30 cm. In the 0–90 cm soil layer of *Pinus tabuliformis* forestland, the cumulative percentage of total root biomass density was more than 95% and the cumulative percentage of fine root biomass density reached 100%. In the Laio model, the active soil depth Z_r was identified as a distribution range of more than 95% of root biomass [20]. Thus, Z_r was 90 cm in this study.

We calculated the total roots', fine roots', and coarse roots' percentages of root biomass density along the soil profile every 10 cm to the root biomass density of 0–100 cm, respectively (Table A1). Here we only listed the cumulative percentage of root biomass density in Table 4 for the convenience of identifying the active soil depth Z_r.

Table 5. Cumulative percentage of root biomass density in the soil profile (Unit: %).

Soil Depth (cm)	Total Roots	Fine Roots	Coarse Roots
0–10	6.63	2.02	21.59
10–20	18.93	9.99	47.93
20–30	81.85	85.31	70.59
30–40	86.84	87.87	83.49
40–50	88.36	88.26	88.70
50–60	89.21	88.26	92.31
60–70	90.00	88.80	93.92
70–80	91.09	89.35	96.72
80–90	99.81	100.00	99.20
90–100	100.00	100.00	100.00

4.1.3. Analysis of Other Conditions in the Study Area

In the Laio model, temporal dynamics of soil moisture are modeled at a point without consideration of the effects due to the lateral moisture contribution [57]. In this study, the sample plot was flat. In addition, the infiltration in forestland on the Loess Plateau is dominated by vertical infiltration. Therefore, soil infiltration satisfied the hypothesis of the Laio model. The groundwater depth near the sample plot was 160 m, resulting in no interaction between the active soil layer and groundwater, which satisfied the Laio model assumption. The study area has a temperate continental monsoon climate. Soil evaporation and plant transpiration are closely related with the soil moisture content, satisfying the hypothesis that soil water loss is related with soil water content in the Laio model. Overall, all the assumptions of the Laio model were satisfied in the study area, thus, the model could be used to simulate soil moisture dynamics in the study area.

4.2. Stochastic Simulation of Soil Moisture in Active Soil Layer

4.2.1. Soil Moisture Dynamics of Active Soil Layer

According to the variation of monthly average soil moisture in 2005–2015 growing seasons (April to October) (Figure 3), the change trend of soil moisture in *Pinus tabuliformis* forestland was closely related to rainfall changes. Generally, we consider 80% of the field capacity as the starting point of plant water stress. When the soil moisture is less than 80% of the field capacity, and more than 60% of the field capacity, plants are under slight water stress. A small amount (1.30%) of the monthly average soil moisture of *Pinus tabuliformis* forestland in the period of 2005–2015 growing seasons was beyond the field capacity, and 9.09% was free of water stress. The months in which Chinese pine forests suffered slight water stress accounted for 29.87% of all observed months in the 2005–2015 growing seasons. Thus, Chinese pine forests were under water stress most of the time, and the soil water deficit may influence plant growth.

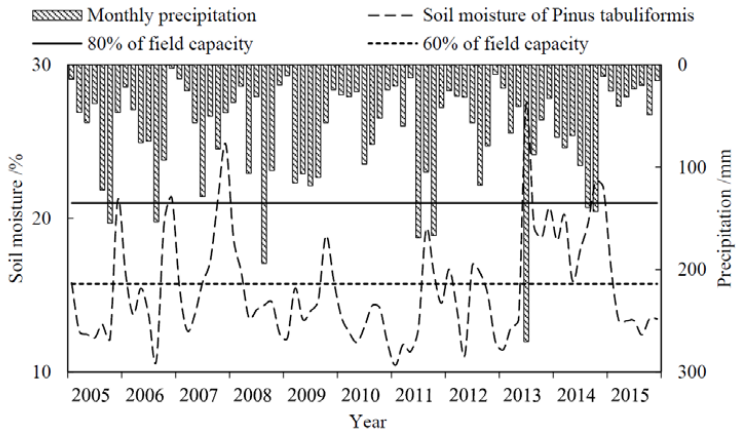

Figure 3. Monthly average soil moisture in *Pinus tabuliformis* Plantation in 2005–2015 growing seasons.

4.2.2. Soil Moisture Simulation Results and Model Evaluation in the Calibration Period

Based on observed soil moisture θ and the genetic algorithm method optimizing six parameters concerning soil, plants, and precipitation in the Laio model, the optimum parameters for *Pinus tabuliformis* forestland in growing seasons in our study area were obtained (Table 6).

Table 6. Optimum model parameter values obtained by a genetic algorithm approach.

	Parameters	Calibration Period	Validation Period
Soil	Soil porosity n	0.5370	0.5073
	Soil porosity distribution parameter β	12.0476	12.0476
	Active soil depth Z_r (cm)	90.0000	90.0000
	Saturated hydraulic conductivity K_s (cm/d)	44.6200	44.6200
	Hygroscopic coefficient s_h	0.1081	0.1081
	Wilting coefficient s_w	0.1629	0.1629
	Critical soil moisture below which plant undergoes water stress s^*	0.3048	0.3048
	Field capacity s_{fc}	0.6683	0.6683
	Soil evaporation at wilting point E_w (cm)	0.0100	0.0100
Plant	Canopy interception threshold Δ (cm)	0.2000	0.1990
	Maximum evapotranspiration rate E_{max} (cm)	0.2134	0.1765
Precipitation	Average rainfall depth α (cm/d)	0.7059	0.6639
	Average rainfall frequency λ (d)	0.3224	0.3205

Using optimum parameters in the calibration period in Table 6, PDF $p(s)$ (Figure 4a) and CDF $P(s)$ (Figure 4b) in the calibration period were obtained ($\chi^2 = 4.5266 < \chi^2_{0.10}(5) = 15.0863$).

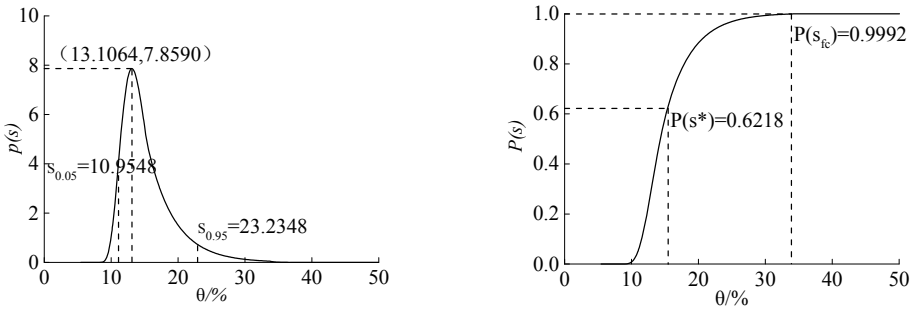

(**a**) (**b**)

Figure 4. PDF (**a**) and CDF (**b**) of soil moisture in the calibration period. (**a**) PDF of soil moisture; (**b**) CDF of soil moisture.

In Figure 4a, the single peak curve $p(s)$ peaked at the point θ = 13.11%, indicating that soil moisture values were most dense in the vicinity of 13.11%. The 90% confidence interval of the simulation results of θ was [10.95%, 23.23%]. Figure 4b showed that the probability of θ between s^* and s_{fc} was 0.3774 and the probability of θ greater than s_{fc} was 0.0008. Simulation results showed that Chinese pine forests in the study area were often affected by water stress, and soil moisture was rarely above the field capacity. Simulation results were consistent with the soil moisture realities of Chinese pine forests in the study area in calibration period (Figure 5).

In the calibration period, observed soil moisture θ ranging from 7.96% to 27.05% was divided into six groups in the interval of 3.18%. We divided the simulated soil moisture into the same groups as the observed soil moisture. In the same soil moisture grouping, the differences between the observation frequency and the simulation probability in the calibration period were compared (Figure 6).

According to Figure 6, the maximum value of the observed frequency $f(\theta)$ in the calibration period was 0.4501, while the maximum simulated probability was 0.4368. The fitting curves both peaked in the group of 11.14–14.32%, which corresponded to the peak position of $p(s)$ (Figure 4a). The observed and simulated θ of *Pinus tabuliformis* forestland in the calibration period both mainly concentrated

(observed values' frequency was more than 0.10) from 11.14% to 20.69%, which was consistent with the 90% confidence interval of $p(s)$ [10.95%, 23.23%] (Figure 4a).

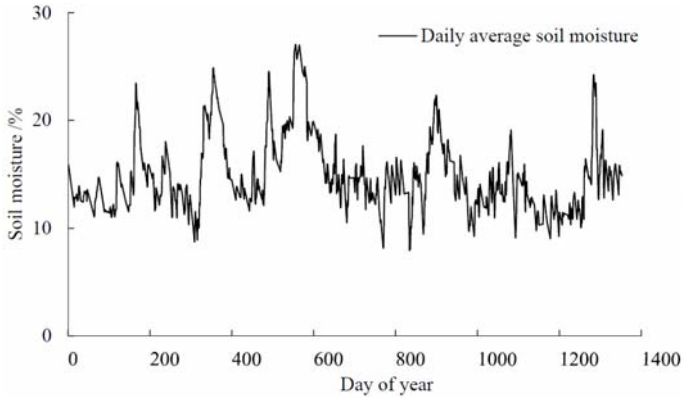

Figure 5. Daily average soil moisture in the calibration period.

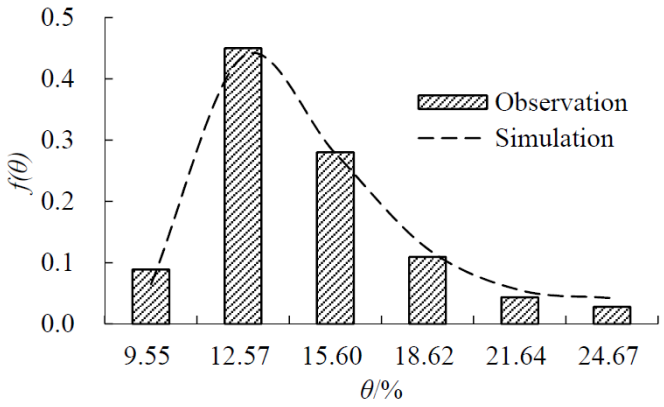

Figure 6. Probability distribution of observed and simulated θ in calibration period.

Numerical characteristics of the observed and simulated soil moisture θ of the 0–90 cm soil layer in *Pinus tabuliformis* forestland during the calibration period (2005–2011) were analyzed. Statistics were indicated with items including upper quartile $\theta_{0.25}$, median $\theta_{0.50}$, lower quartile $\theta_{0.75}$, mean value $E(\theta)$, and standard deviation $\sigma(\theta)$ (Table 7).

Table 7. Statistical characteristics of soil moisture θ in the calibration period (Unit: %).

Statistical Items	Observation	Simulation	Relative Error
$\theta_{0.25}$	12.50	12.64	1.12
$\theta_{0.50}$	14.02	14.31	2.07
$\theta_{0.75}$	16.03	17.01	6.11
$E(\theta)$	14.77	15.33	3.79
$\sigma(\theta)$	3.43	3.89	13.41

Relative errors between some critical items of the simulated and observed θ were mostly within 7%, except for standard deviation. Consistency index J was 0.9906 in the calibration period, suggesting that the model credibility was high and the simulation results were consistent with reality.

Above all, according to the consistency of PDF and CDF with the soil moisture realities of Chinese pine forests in the study area, a comparison of the observed and simulated $f(\theta)$ in the same θ grouping, and a comparison of numerical characteristics of the observed and simulated θ in calibration period,

the Laio model could simulate the soil moisture dynamics in the active soil layer quite well in a typical *Pinus tabuliformis* forestland during the calibration period in the study area.

4.2.3. Soil Moisture Simulation Results and Model Evaluation in the Validation Period

In order to further verify the feasibility of the Laio model in the study area, we input experimental parameters in the growing seasons of 2012–2015 and optimum parameters in the calibration period. PDF $p(s)$ (Figure 7a) and CDF $P(s)$ (Figure 7b) of s in the validation period were obtained ($\chi^2 = 4.4366 < \chi^2_{0.10}(6) = 16.8119$).

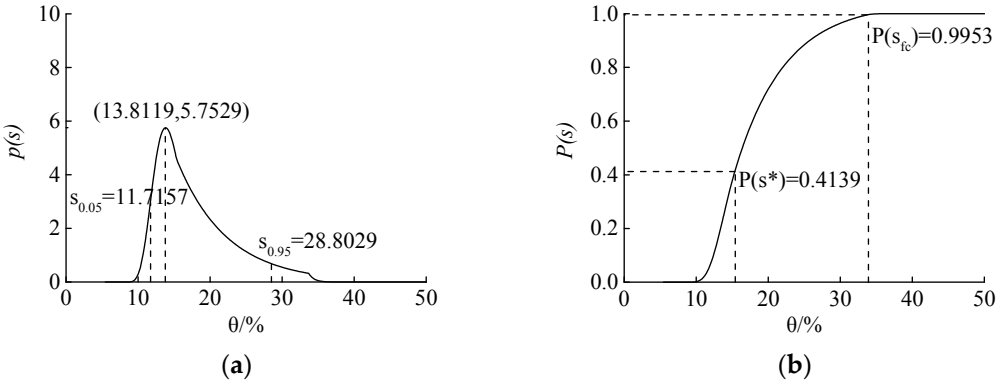

Figure 7. PDF (**a**) and CDF (**b**) of the soil moisture during the validation period. (**a**) PDF of soil moisture; (**b**) CDF of soil moisture.

In Figure 7a, the single peak curve $p(s)$ peaked at the point $\theta = 13.81\%$, indicating that soil moisture values were most dense in the vicinity of 13.81%. The 90% confidence interval of the simulation results of θ was [11.72%, 28.80%]. Figure 7b showed that the probability of θ between s^* and s_{fc} was 0.5814 and the probability of θ greater than s_{fc} was 0.0047. Simulation results were consistent with the soil moisture realities of Chinese pine forests in the study area in the validation period (Figure 8).

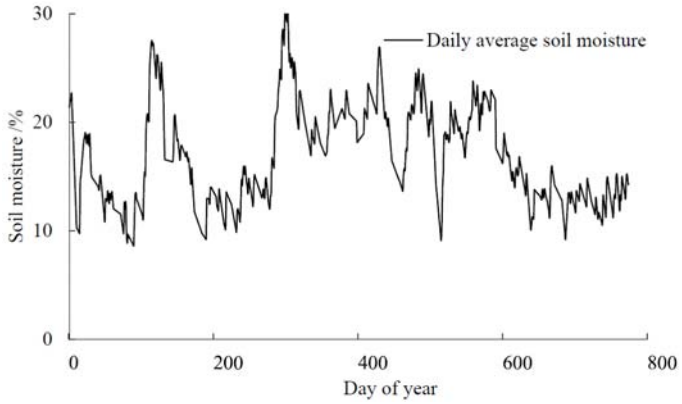

Figure 8. Daily average soil moisture in the validation period.

In the validation period, the observed θ ranging from 8.61% to 30.07% was divided into seven groups in the interval of 3.07%. We also divided the simulated θ into the same groups as the observed θ, and compared the observation frequency and the simulation probability in the validation period (Figure 9).

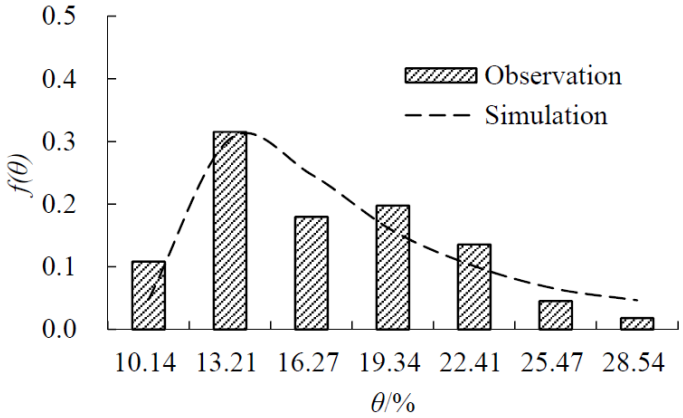

Figure 9. Probability distribution of observed and simulated θ in validation period.

According to Figure 9, the maximum value of the observed frequency $f(\theta)$ in the calibration period was 0.3152, while the maximum simulated probability was 0.3045. The fitting curves both peaked in the group of 11.68–14.74%, which corresponded to the peak position of $p(s)$ (Figure 7a). The observed and simulated θ of *Pinus tabuliformis* forestland in the validation period both mainly concentrated (observed values' frequency was more than 0.10) from 11.68% to 23.94%, which was consistent with the 90% confidence interval of $p(s)$ [11.72%, 28.80%] (Figure 7a).

Numerical characteristics of the observed and simulated soil moisture θ of the 0–90 cm soil layer in *Pinus tabuliformis* forestland during the validation period (2012–2015) were analyzed. Comparisons of the statistical items are shown in Table 8.

Table 8. Statistical characteristics of soil moisture θ in validation period (Unit: %).

Statistical Items	Observation	Simulation	Relative Error
$\theta_{0.25}$	13.10	13.82	5.50
$\theta_{0.50}$	15.93	16.40	2.95
$\theta_{0.75}$	20.35	20.70	1.72
$E(\theta)$	16.71	17.83	6.70
$\sigma(\theta)$	4.50	4.28	4.89

Relative errors between some critical items of the simulated and observed θ were mostly within 7%. Consistency index J was 0.9155 in the calibration period, suggesting that the model credibility was high and the simulation results were consistent with reality.

Above all, according to consistency of PDF and CDF with the soil moisture realities of Chinese pine forests in the study area, the comparison of the observed and simulated $f(\theta)$ in the same θ grouping, and the comparison of numerical characteristics of observed and simulated θ in validation period, the Laio model could simulate soil moisture dynamics in the active soil layer in typical vegetation *Pinus tabuliformis* forestland quite well during the validation period in the study area.

4.3. Analysis of Impact Factors on the Model Results

4.3.1. Impact of Different Sampling Intervals on the Model Results

Based on the genetic algorithm method and the observed soil moisture data at the sampling intervals of 10 days and 30 days, six parameters concerning soil, plants, and precipitation in the Laio model were optimized, respectively. Optimum parameters for soil moisture data at the sampling intervals of 10 days and 30 days were the same, and these parameters were the same as the optimum parameters of the daily soil moisture, except for E_{max} in the validation period, which is 0.1865, slightly higher than E_{max} optimized by the daily soil moisture. Thus, the model results for the soil moisture

data at the sampling intervals of 10 days and 30 days were the same. This also indicated that the sampling interval has a certain impact on the model calibration parameters, however, the change in the parameters due to different sampling intervals was not large.

Using optimum parameters in the calibration and validation periods, PDF $p(s)$ and CDF $P(s)$ at a sampling interval of 10 days (calibration period: $\chi^2 = 1.6740 < \chi^2_{0.10}(5) = 15.0863$; validation period: $\chi^2 = 6.3915 < \chi^2_{0.10}(5) = 13.2767$) and PDF $p(s)$ and CDF $P(s)$ at sampling interval of 30 days (calibration period: $\chi^2 = 1.5776 < \chi^2_{0.10}(5) = 11.3449$; validation period: $\chi^2 = 0.9786 < \chi^2_{0.10}(3) = 9.2103$) were obtained. Since the optimum parameters of the two sampling intervals were the same, PDF $p(s)$ (Figure 10) and CDF $P(s)$ (Figure 11) calculated by the Laio model were also the same.

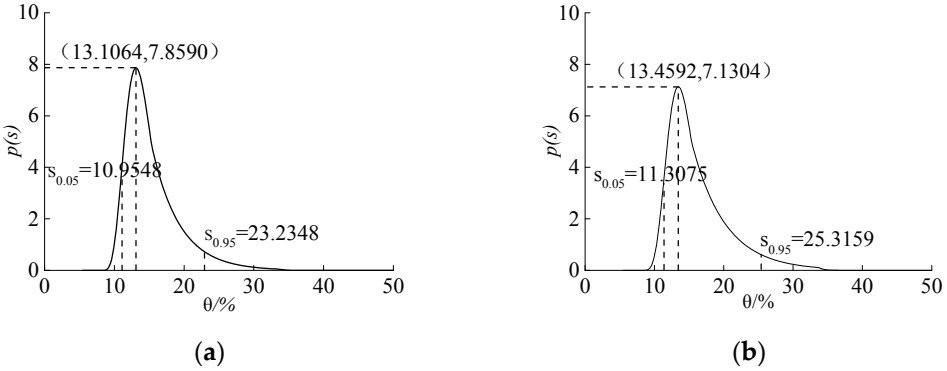

(**a**) (**b**)

Figure 10. PDF of soil moisture at different sampling intervals. (**a**) Calibration period; (**b**) Validation period.

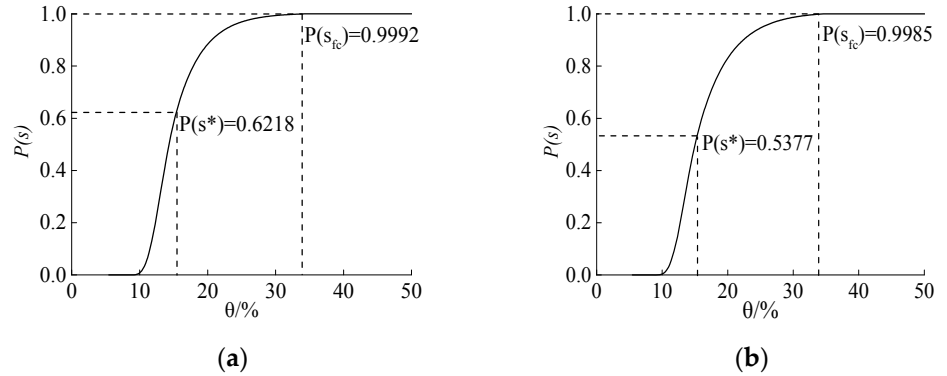

(**a**) (**b**)

Figure 11. CDF of soil moisture at different sampling intervals. (**a**) Calibration period; (**b**) Validation period.

According to Figure 10a, in the calibration period, the single peak curve $p(s)$ peaked at the point $\theta = 13.11\%$. The 90% confidence interval of simulation results of θ was [10.95%, 23.23%]. Figure 11a showed that the probability of θ between s^* and s_{fc} was 0.3774 and the probability of θ greater than s_{fc} was 0.0008. In the validation period, according to Figure 10b, the single peak curve $p(s)$ peaked at the point $\theta = 13.46\%$. The 90% confidence interval of simulation results of θ was [11.31%, 25.32%]. Figure 11b shows that the probability of θ between s^* and s_{fc} was 0.4608 and the probability of θ greater than s_{fc} was 0.0015. The simulation results were consistent with the soil moisture realities of Chinese pine forests in the study area (Figure 12).

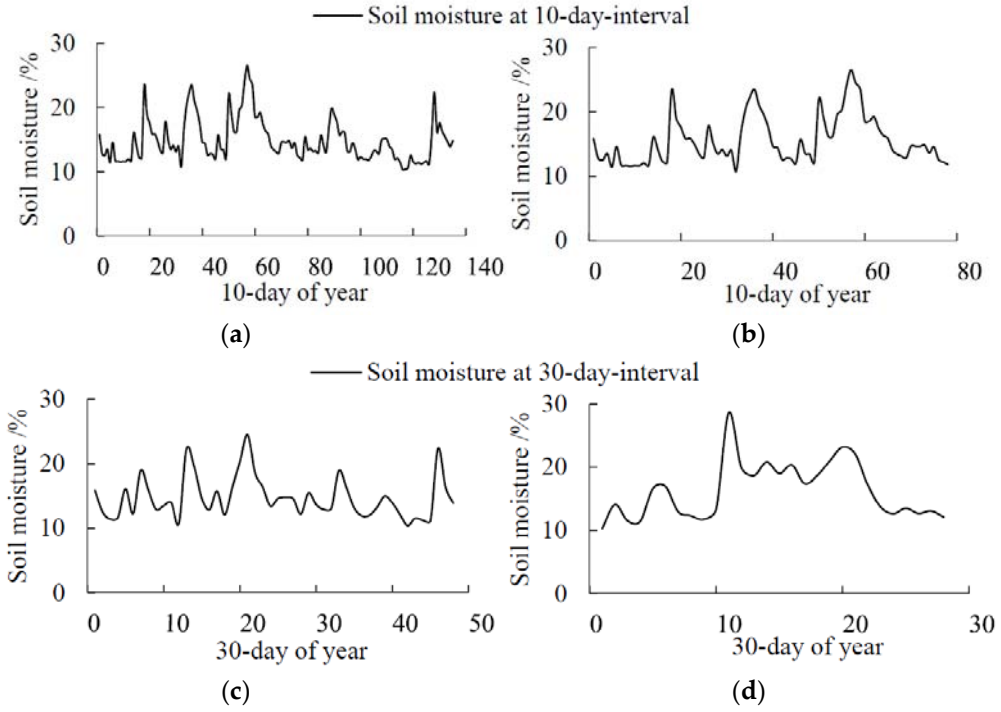

Figure 12. Soil moisture at different sampling intervals. (**a**) 10-day sampling interval in the calibration period; (**b**) 10-day sampling interval in the validation period; (**c**) 30-day sampling interval in the calibration period; (**d**) 30-day sampling interval in the validation period.

When the soil moisture sampling interval was 10 days, the observed soil moisture θ ranging from 10.32% to 26.53% was divided into six groups in the interval of 2.70% in the calibration period; while in the validation period the observed θ, ranging from 9.65% to 28.58%, was divided into six groups in the interval of 3.16%. When the soil moisture sampling interval was 30 days the observed θ, ranging from 10.39% to 24.46%, was divided into six groups in the interval of 2.35% in the calibration period; however, in the validation period the observed θ ranging from 10.29% to 28.58%, was divided into four groups in the interval of 4.57%. We divided the simulated soil moisture into the same groups as the observed soil moisture. In the same soil moisture groups, the differences between the observation frequency and the simulation probability in both the calibration period and the validation period were compared (Figure 13).

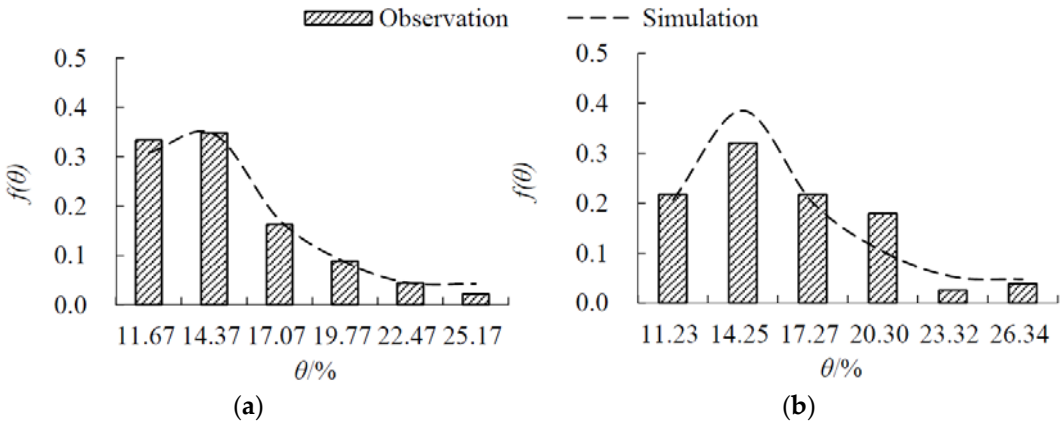

Figure 13. *Cont.*

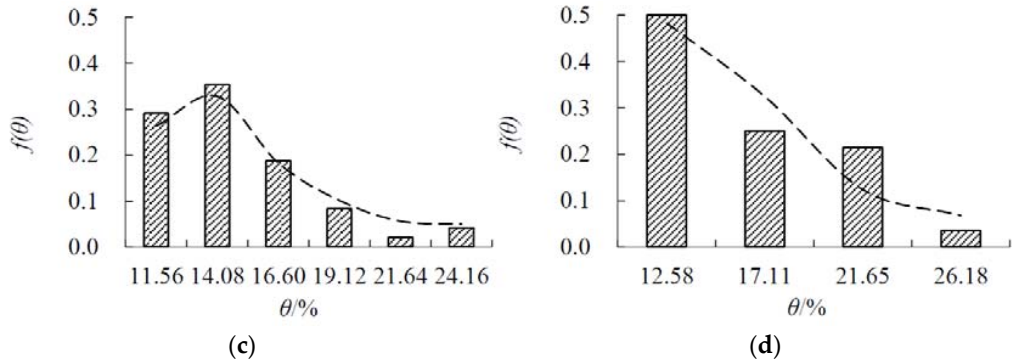

Figure 13. Probability distribution of the observed and simulated θ at different sampling intervals. (**a**) 10-day sampling interval in the calibration period; (**b**) 10-day sampling interval in the validation period; (**c**) 30-day sampling interval in the calibration period; (**d**) 30-day sampling interval in the validation period.

According to Figure 13, when the soil moisture sampling interval was 10 days, the error of the maximum value of statistical frequency $f(\theta)$ between simulated and observed θ in the calibration period was 0.75% (Figure 13a); while in the validation period, the error was 20.25% (Figure 13b). When soil moisture sampling interval was 30 days, the error of the maximum value of statistical frequency $f(\theta)$ between the simulated and observed θ in the calibration period was 7.30% (Figure 13c) while, in the validation period, the error was 3.41% (Figure 13d). In the calibration and validation periods, the peak of the simulated probability and observed frequency at two soil moisture sampling intervals both distributed in the same interval; more precisely, [13.02%, 15.72%] for the 10-day sampling interval (Figure 13a) and [12.74%, 15.08%] for the 30-day sampling interval (Figure 13c) in the calibration period, [12.81%, 15.96%] for the 10-day sampling interval (Figure 13b) and [10.29%, 14.86%] for the 30-day sampling interval (Figure 13d) in the validation period corresponded to the peak position of $p(s)$ in the same period. The observed and simulated θ of *Pinus tabuliformis* forestland in the calibration period both mainly concentrated (observed values' frequency was more than 0.10) from 10.32% to 18.42%, which was consistent with the 90% confidence interval of $p(s)$ [10.95%, 23.23%] (Figure 10a). The observed and simulated θ of *Pinus tabuliformis* forestland in the validation period both mainly concentrated from 9.65% to 22.27%, which was consistent with the 90% confidence interval of $p(s)$ [11.31%, 25.32%] (Figure 10b).

Numerical characteristics of observed and simulated soil moisture θ at sampling intervals of 10 days and 30 days in *Pinus tabuliformis* forestland during the calibration period (2005–2011) and the validation period (2012–2015) are analyzed (Table 9).

Table 9. Statistical characteristics of soil moisture θ at different sampling intervals (Unit: %).

Statistical Items	Calibration Period			Validation Period		
	Observation	Simulation	Relative Error	Observation	Simulation	Relative Error
10-day sampling interval						
$\theta_{0.25}$	12.43	12.64	1.69	12.86	13.12	2.02
$\theta_{0.50}$	13.95	14.31	2.58	14.80	15.01	1.42
$\theta_{0.75}$	16.21	17.01	4.94	18.93	18.23	3.70
$E(\theta)$	14.88	15.33	3.02	16.18	16.23	0.31
$\sigma(\theta)$	3.35	3.89	16.12	4.18	4.38	4.78
30-day sampling interval						
$\theta_{0.25}$	12.25	12.64	3.18	12.67	13.12	3.55
$\theta_{0.50}$	13.91	14.31	2.88	15.31	15.01	1.96
$\theta_{0.75}$	16.13	17.01	5.46	19.23	18.23	5.20
$E(\theta)$	14.73	15.33	4.07	16.27	16.23	0.25
$\sigma(\theta)$	3.23	3.89	20.43	4.46	4.38	1.79

With the increase of sampling interval days, the error between the observed and simulated values increased slightly, but most of the error values were less than 20%, indicating that the model simulation results were reliable. When the soil moisture sampling interval was 10 days, the consistency index J is 0.9888 in the calibration period and 0.8288 in the validation period; when the soil moisture sampling interval was 30 days, J is 0.9611 in the calibration period and 0.8625 in the validation period, suggesting that the model credibility was high and the simulation results were consistent with reality.

Above all, according to consistency of PDF and CDF with the soil moisture realities of Chinese pine forests in the study area, the comparison of the observed and simulated $f(\theta)$ in the same θ grouping, and the comparison of numerical characteristics of the observed and simulated θ in the calibration and validation periods at two sampling intervals, the data sampling interval had some effect on the simulation results. With the increase of the sampling interval, the difference between the observed and simulated values increased, suggesting that the shorter the sampling interval was, the closer the simulation results were to reality.

4.3.2. Model Sensitivity to Parameter Changes

Optimum parameters calibrated by daily soil moisture in the calibration period were taken as an example. According to the sensitivity analysis, the parameters were classified into weakly-, medium-, and strongly-sensitive parameters.

1. If the change of the $p(s)$ peak value was almost 0 before and after parameter adjustments, these parameters were classified as weakly-sensitive parameters. Weakly-sensitive parameters included β, K_s, s_h, and E_w. Adjustments of these parameters had little effect on the peak value, the 90% confidence interval, and the curve shape of $p(s)$, indicating that the Laio model was weakly sensitive to these parameters.
2. If the change of the $p(s)$ peak value was more than 0 and less than 10% of the original results before and after parameter adjustments, these parameters were classified as medium-sensitive parameters. Medium-sensitive parameters included n, Z_r, s^*, s_w, s_{fc}, and Δ. These parameters had a certain degree of effect on $p(s)$. s_w and s^* influenced the peak value of $p(s)$; s_{fc} mainly affected the 90% confidence interval of $p(s)$; n, Z_r, and Δ had an effect on both the peak value and 90% confidence interval of $p(s)$.
3. If the change of the $p(s)$ peak value was more than 10% of the original results before and after parameter adjustments, these parameters were classified as strongly-sensitive parameters. Strongly-sensitive parameters included E_{max}, α, and λ. Adjusting any one of the three parameters had a significant effect on $p(s)$. Parameter adjustments mainly influenced the 90% confidence interval of $p(s)$. With the increase of E_{max}, the peak value of $p(s)$ increased, while the peak position of $p(s)$ slightly decreased and the range of the 90% confidence interval decreased (Figure 14a), suggesting that with the increase of evapotranspiration, soil moisture content decreased and the probability concentrated in the low level of soil moisture content increased. With the increase of α, the peak value of $p(s)$ decreased rapidly, while the peak position of $p(s)$ increased slightly and the range of the 90% confidence interval increased (Figure 14b). With the increase of λ, the peak value of $p(s)$ decreased, while the peak position of $p(s)$ increased slightly and the range of the 90% confidence interval increased (Figure 14c). The change of $p(s)$ after the adjustment of α and λ indicated that with the increase of rainfall depth and rainfall frequency, soil moisture content increased and the probability concentrated at a high level of soil moisture content increased.

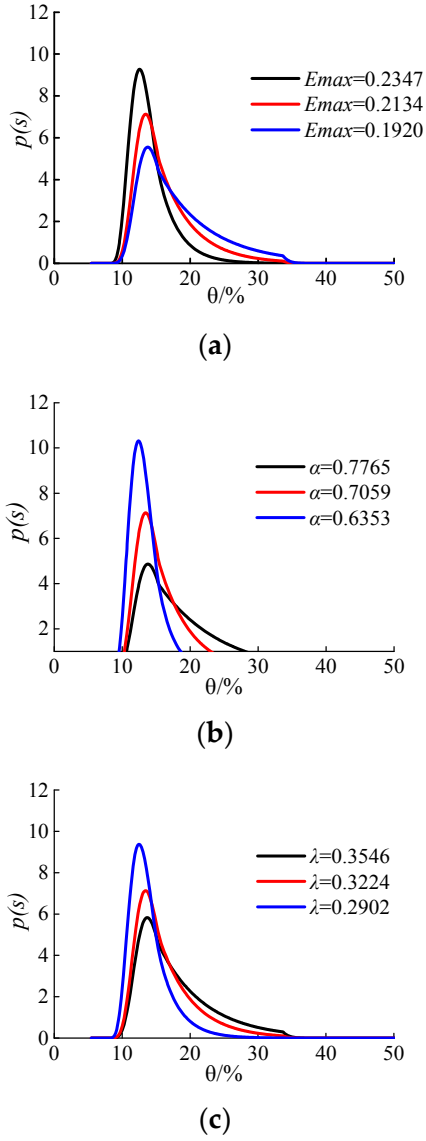

Figure 14. Influence of the strongly-sensitive parameters on the Laio model results. (**a**) Influence of E_{max} on model results; (**b**) Influence of α on model results; (**c**) Influence of λ on model results.

5. Discussion

According to comparisons of statistical items, relative errors between observed and simulated values were less than 7%, except for the standard deviation in the calibration period. With regard to standard deviation, most of the dispersions of the simulation results in the calibration and validation periods were larger than those of the observations. The cause of the high relative error of standard deviation in the calibration period may be because the inputs of the Laio model, including rainfall depth, rainfall frequency, and the maximum evapotranspiration rate of *Pinus tabuliformis* forestland, were the average of many years' data, and the outputs of the Laio model showed a steady state of soil moisture, leading to the fact that we could just approximately simulate the variation of factors.

The trend of observed frequency and simulated probability of soil moisture at different sampling intervals was almost the same except in one group in the validation period at each sample interval (group center value was 25.47% for daily soil moisture, 20.30% for 10-day sampling interval soil moisture and 21.65% for 30-day sampling interval soil moisture). Frequencies of observed soil moisture in these groups were higher than probabilities of simulated results. Generally, soil moisture probability

is subject to normal distribution, and the probability distribution curve only has one peak. According to Figure 3, a lot of precipitation concentrated in growing seasons of 2013–2014, leading to higher soil moisture values in 2013–2014. It made the observed soil moisture frequency higher than normal conditions, especially in high-level soil moisture groups. Thus, the relatively high frequencies of observed soil moisture in some groups in the validation period were only an occasional fluctuation caused by more precipitation.

By changing parameters, including soil type, rainfall frequency, rainfall depth, evapotranspiration, and so on, Laio [20] acquired 12 kinds of PDF representing 12 environmental conditions of different soil depths and climate types. Among these environmental conditions, the PDF, under the condition that loam soil with Z_r = 90 cm, α = 1.5 cm, λ = 0.2, and E_{max} = 0.45 cm/d, complied with the curve of *Pinus tabulaeformis* forestland on the Loess Plateau in this study. This was because the climate and vegetation conditions on the Loess Plateau were similar to the conditions in Laio's study.

Compared with the daily soil moisture, the soil moisture at sampling intervals of 10 days and 30 days might lose some information about soil moisture fluctuations, but they still could reflect the overall change trend of θ during growing seasons. The PDF of the Laio model showed the statistic characteristics and concentration trend of θ. In the long term, the instantaneous fluctuation of soil moisture will not change the overall trend of soil moisture during the growing season, thus, the sampling interval had little impact on the model application. The soil moisture data of different sampling intervals had a certain influence on the model simulation results by influencing values of the optimum parameters. The shorter the sampling interval was, the closer the simulation results were to reality. According to comparisons of the frequency distribution curves of the observed soil moisture at different sampling intervals, the frequency distribution curve of the observed soil moisture at a 10-day sampling interval was similar to the frequency distribution curve of the daily observed soil moisture. However, the details of the soil moisture overall trend, showed by a frequency distribution curve of observed soil moisture at a 30-day sampling interval, was insufficient. When applying the Laio model in areas that lack a high frequency of monitored soil moisture data, it was suggested to use soil moisture data with a sampling interval of no more than 10 days to calibrate the model so as to ensure that the observed soil moisture was closer to reality.

6. Conclusions

This study investigated the applicability of the Laio soil moisture dynamics stochastic model in *Pinus tabuliformis* forestland, which is the typical forest ecosystem on the Loess Plateau of China, studied the model sensitivity to parameters, and analyzed the impact of the data sampling interval on model calibration and simulation results, providing a theoretical basis for choosing an appropriate data sampling interval in the application of the model.

The Laio model had good applicability in a typical ecosystem of *Pinus tabuliformis* forestland on the Loess Plateau. In the application process of the Laio model in the study area, it was recommended to use soil moisture data with a sampling interval of no more than 10 days to calibrate the model so as to reduce the loss of soil moisture fluctuation information due to a long sampling interval. Among Laio model parameters, the Laio model showed high sensitivity to the maximum evapotranspiration rate E_{max}, average rainfall depth α, and average rainfall frequency λ. Thus, in order to ensure the stability and reliability of the model simulation results, more attention should be paid to better estimate their values in the application of the model.

When applying the model, it is better to choose a longer period as a validation period, and we should avoid choosing years in which rainfall amount is abnormal. There are still some limits which influence the accuracy of the model. Some works need to be done to make the model more suitable for forestland. New parameters representing special hydrological characteristics of forestland can be added, such as the function of litter layer. Furthermore, intensive research about different age forestlands (young-age forestland, mature forestland and over-mature forestland) could be conducted.

Acknowledgments: This study was funded by The National Key Research and Development Program of China (No. 2016YFC0501704), National Natural Science Funds of China (No. 31470638) and Beijing Collaborative Innovation Center for Eco-Environmental Improvement with Forestry and Fruit Trees (PXM2016_014207_000038). This research was supported by CFERN & BEIJING TECHNO SOLUTIONS Award Funds on excellent academic achievements. Many thanks are given to the anonymous reviewers and the editors for their help. Thanks are also due to Yu-Bo Sun, Hang-Qi Duan, Xiao-Xian Wang, and Yu-Jie Bai for their help during the field survey and data processing.

Author Contributions: Yi-Fang Chang and Hua-Xing Bi conceived and designed the experiments; Yi-Fang Chang, Zhi-Cai Cai, Dan Wang, and Hua-Sen Xu performed the experiments; Yi-Fang Chang and Qing-Fu Ren analyzed the data; Qing-Fu Ren and Wen-Chao Liao contributed reagents/materials/analysis tools; Yi-Fang Chang wrote the paper; Yi-Fang Chang, Hua-Xing Bi and Hua-Sen Xu revised the paper.

Conflicts of Interest: The authors declare no conflict of interest. The founding sponsors had no role in the design of the study; in the collection, analyses, or interpretation of data; in the writing of the manuscript; or in the decision to publish the results.

Appendix A

We calculated the total roots', fine roots', and coarse roots' percentages of root biomass density along the soil profile every 10 cm to the root biomass density of 0–100 cm respectively (Table A1).

Table A1. Root biomass density along the soil profile (Unit: g).

Soil Depth (cm)	Total Roots	Fine Roots	Coarse Roots
0–10	4.21	0.98	3.23
10–20	7.81	3.87	3.94
20–30	39.96	36.57	3.39
30–40	3.17	1.24	1.93
40–50	0.97	0.19	0.78
50–60	0.54	0.00	0.54
60–70	0.50	0.26	0.24
70–80	0.69	0.27	0.42
80–90	5.54	5.17	0.37
90–100	0.12	0.00	0.12

References

1. Guo, Z.S. *Theory and Practice on Soil Water Carrying Capacity for Vegetation*, 1st ed.; Science Press: Beijing, China, 2014; Volume 1, pp. 10–16. ISBN:978-7-03-040468-8.
2. Feng, Q.; Zhao, W.; Qiu, Y.; Zhao, M.; Zhong, L. Spatial Heterogeneity of Soil Moisture and the Scale Variability of Its Influencing Factors: A Case Study in the Loess Plateau of China. *Water* **2013**, *5*, 1228. [CrossRef]
3. Liu, Y.; Zhao, W.; Zhang, X.; Fang, X. Soil Water Storage Changes within Deep Profiles under Introduced Shrubs during the Growing Season: Evidence from Semiarid Loess Plateau, China. *Water* **2016**, *8*, 475. [CrossRef]
4. Yin, Z.; Feng, Q.; Zou, S.; Yang, L. Assessing Variation in Water Balance Components in Mountainous Inland River Basin Experiencing Climate Change. *Water* **2016**, *8*, 472. [CrossRef]
5. Hemp, A. Climate change and its impact on the forests of Kilimanjaro. *Afr. J. Ecol.* **2009**, *47*, 3–10. [CrossRef]
6. Alexandridis, T.K.; Cherif, I.; Bilas, G.; Almeida, W.G.; Hartanto, I.M.; van Andel, S.J.; Araujo, A. Spatial and Temporal Distribution of Soil Moisture at the Catchment Scale Using Remotely-Sensed Energy Fluxes. *Water* **2016**, *8*, 32. [CrossRef]
7. Legates, D.R.; Mahmood, R.; Levia, D.F.; DeLiberty, T.L.; Quiring, A.M.; Houser, C.; Nelson, F.E. Soil moisture: A central and unifying theme in physical geography. *Prog. Phys. Geogr.* **2010**, *35*, 65–86. [CrossRef]
8. Hu, J.; Lü, Y.H. Research progress on stochastic soil moisture dynamic model. *Prog. Geogr.* **2015**, *34*, 389–400. [CrossRef]
9. Walker, J.P.; Willgoose, G.R.; Kalma, J.D. One-dimensional soil moisture profile retrieval by assimilation of near-surface observations: A comparison of retrieval algorithms. *Adv. Water Resour.* **2001**, *24*, 631–650. [CrossRef]

10. Crow, W.T.; Kusta, W.P.; Prueger, J.H. Monitoring root-zone soil moisture through the assimilation of a thermal remote sensing-based soil moisture proxy into a water balance model. *Remote Sens. Environ.* **2008**, *112*, 1268–1281. [CrossRef]
11. Montzka, C.; Moradkhani, H.; Weihermüller, L.; Franssen, H.J.H.; Canty, M.; Vereecken, H. Hydraulic parameter estimation by remotely-sensed top soil moisture observations with the particle filter. *J. Hydrol.* **2011**, *399*, 410–421. [CrossRef]
12. Yan, H.X.; DeChant, C.M.; Moradkhani, H. Improving soil moisture profile prediction with the particle filter-Markov chain Monte Carlo method. *IEEE Trans. Geosci. Remote* **2015**, *53*, 6134–6147. [CrossRef]
13. Feddes, R.A.; Kabat, P.; Van Bakel, P.J.T.; Bronswijk, J.J.B.; Halbertsma, J. Modelling soil water dynamics in the unsaturated zone—State of the art. *J. Hydrol.* **1988**, *100*, 69–111. [CrossRef]
14. Rodriguez-Iturbe, I.; Entekhabi, D.; Bras, R.L. Nonlinear dynamics of soil moisture at climate scales: 1. stochastic analysis. *Water Resour. Res.* **1991**, *27*, 1899–1906. [CrossRef]
15. Rodriguez-Iturbe, I.; Porporato, A.; Ridolfi, L.; Isham, V.; Cox, D.R. Probabilistic modeling of water balance at a point: The role of climate, soil and vegetation. *Proc. R. Soc. Lond. A* **1999**, *455*, 3789–3805. [CrossRef]
16. Ren, Q.F.; Yan, D.H.; Mu, W.B.; Pei, H.W. Stochastic model of irrigated farmland soil moisture dynamics at a point in piedmont of Mount Taihang. *Trans. Chin. Soc. Agric. Mach.* **2015**, *46*, 131–141. [CrossRef]
17. Liu, H.; Zhao, W.Z. Advances in research on soil moisture probability density functions obtained from models for stochastic soil moisture dynamics. *Adv. Water Sci.* **2006**, *17*, 894–904. [CrossRef]
18. Eagleson, P.S. Climate, soil, and vegetation: 6. dynamics of the annual water balance. *Water Resour. Res.* **1978**, *14*, 749–763. [CrossRef]
19. Huang, L.; Zhang, Z.S.; Chen, Y.L. Probabilistic modelling of soil moisture dynamics in a revegetated desert area. *J. Desert Res.* **2013**, *33*, 568–573. [CrossRef]
20. Laio, F.; Porporato, A.; Ridolfi, L.; Rodriguez-Iturbe, I. Plants in water-controlled ecosystems: Active role in hydrologic processes and response to water stress: II. Probabilistic soil moisture dynamics. *Adv. Water Resour.* **2001**, *24*, 707–723. [CrossRef]
21. Yao, S.X.; Zhang, T.H.; Zhao, C.C. Analysis of soil moisture dynamics and its probability density function simulation in Horqin sand land. *Adv. Water Sci.* **2013**, *24*, 62–72. [CrossRef]
22. Ridolfi, L.; D'Odorico, P.; Porporato, A.; Rodriguez-Iturbe, I. Stochastic soil moisture dynamics along a hillslope. *J. Hydrol.* **2003**, *272*, 264–275. [CrossRef]
23. Laio, F. A vertically extended stochastic model of soil moisture in the root zone. *Water Resour. Res.* **2006**, *420*, 355–363. [CrossRef]
24. Rodriguez-Iturbe, I.; D'Odorico, P.; Laio, F.; Ridolfi, L.; Tamea, S. Challenges in humid land ecohydrology: Interactions of water table and unsaturated zone with climate, soil, and vegetation. *Water Resour. Res.* **2007**, *43*, 1–8. [CrossRef]
25. Laio, F.; Tamea, S.; Ridolfi, L.; D'Odorico, P.; Rodriguez-Iturbe, I. Ecohydrology of groundwater-dependent ecosystems: 1. stochastic water table dynamics. *Water Resour. Res.* **2009**, *45*, 207–213. [CrossRef]
26. Tamea, S.; Laio, F.; Ridolfi, L.; D'Odorico, P.; Rodriguez-Iturbe, I. Ecohydrology of groundwater-dependent ecosystems: 2. stochastic soil moisture dynamics. *Water Resour. Res.* **2009**, *45*, 207–213. [CrossRef]
27. Huang, M.B.; Shao, M.A.; Li, Y.S. A modified stochastic dynamic water balance model and its application: I. model. *J. Hydraul. Eng.* **2000**, *31*, 20–26. [CrossRef]
28. Huang, M.B.; Shao, M.A.; Li, Y.S. A modified stochastic dynamic water balance model and its application II: Model validation. *J. Hydraul. Eng.* **2000**, *31*, 27–33. [CrossRef]
29. Eagleson, P.S. Climate, soil, and vegetation: 1. introduction to water balance dynamics. *Water Resour. Res.* **1978**, *14*, 705–712. [CrossRef]
30. Liu, H.; Zhao, W.Z.; He, Z.B.; Zhang, L.J. The stochastic model of soil moisture dynamics in the grass ecosystem at a point in the Qilian mountainous area. *Sci. China Ser. D Earth Sci.* **2007**, *50*, 1844–1856. [CrossRef]
31. Wang, G.G.; Lü, J.K.; Wei, C.F. Soil moisture dynamics and its stochastic simulation in hilly areas in Sichuan Basin. *China Rural Water Hydropower* **2009**, *11*, 22–26. [CrossRef]
32. Pan, X.Y.; Zhang, L.; Potter, N.J.; Xia, J.; Zhang, Y.Q. Probabilistic model-ling of soil moisture dynamics of irrigated cropland in the North China Plain. *Hydrol. Sci. J.* **2011**, *56*, 123–137. [CrossRef]
33. Pan, X.Y.; Potter, N.J.; Xia, J.; Zhang, L. Hillslope-scale probabilistic characterization of soil moisture dynamics and average water balance. *Hydrol. Process.* **2013**, *27*, 1464–1474. [CrossRef]

34. Rodriguez, I. Ecohydrology: A perspective of climate-soil-vegetation dynamics. *Water Resour. Res.* **2000**, *36*, 3–9. [CrossRef]
35. Laio, F.; Porporato, A.; Ferandez-Illescas, C.P.; Rodriguez-Iturbe, I. Plants in water-controlled ecosystem: Active role in hydrologic processes and response to water stress IV: Discussion of real cases. *Adv. Water Res.* **2001**, *24*, 745–762. [CrossRef]
36. Porporato, A.; D'Odorico, P.; Laio, F.; Ridolfi, L.; Rodriguez-Iturbe, I. Ecohydrology of water-controlled ecosystems. *Adv. Water Res.* **2002**, *25*, 1335–1348. [CrossRef]
37. Pan, X.Y.; Xia, J.; Zhang, L. A review of soil water balance studies based on stochastic soil moisture model. *Resour. Sci.* **2008**, *30*, 460–467. [CrossRef]
38. Porporato, A.; Laio, F.; Ridolfi, L.; Rodriguez-Iturbe, I. Plants in water-con-trolled ecosystems: Active role in hydrologic processes and response to water stress III: Vegetation water stress. *Adv. Water Res.* **2001**, *24*, 725–744. [CrossRef]
39. Cox, D.R.; Miller, H.D. *The Theory of Stochastic Processes*, 1st ed.; Chapman and Hall/CRC: London, UK, 1977; pp. 1–408. ISBN:978-0412151705.
40. Gao, L.B.; Bi, H.X.; Xu, H.S.; Liao, W.C.; Wang, X.Y.; Chang, Y.F.; Chen, J.G. Spatial distribution of soil moisture and soil nutrients and the effects of young apple-soybean intercropping system on soybean in the Loess Plateau of west Shanxi province. *Chin. Agric. Bull.* **2013**, *29*, 37. [CrossRef]
41. Xu, H.S.; Bi, H.X.; Gao, L.B.; Yun, L.; Liao, W.C.; Chang, Y.F. Niche of roots in the economic tree and crop intercropping system in the western Shanxi province of Loess Plateau. *Chin. Agric. Bull.* **2013**, *29*, 70. [CrossRef]
42. Ru, H. *Analysis of Hydrological Characteristics and Functions of Typical Forest Stands in the Loess Plateau Area of Western Shanxi Province*; Beijing Forestry University: Beijing, China, 2015; Volume 50.
43. Zhu, J.Z.; Zhu, Q.K. *The Data Set of Chinese Ecosystem Orientation Observation and Research- Forest Ecosystem Volume (Shanxi Jixian Station 1978–2006)*, 1st ed.; China Agriculture Press: Beijing, China, 2010; p. 17. ISBN:9787109150737.
44. Cheng, D.J.; Zhang, Y.L. *Soil Physics Experiment Guide*, 1st ed.; China Water & Power Press: Beijing, China, 2012; p. 17. ISBN:9787508494319.
45. Li, X.Y.; Bi, H.X.; Zhang, J.J.; Li, J.; Lin, J.J. Study on the validity of soil moisture in Loess Area. *Res. Soil Water Conserv.* **2006**, *13*, 205–211. [CrossRef]
46. Zhang, C.B. *Fundamental and Mechanical Study on Soil Reinforcement and Slope Protection by Woody Plant Roots*; Beijing Forestry University: Beijing, China, 2011; pp. 29–32.
47. Zhang, P. *A Study on Biological Characteristics and Growth Performance of Black Locust Barrow-Crown Clone (Robinia pseudoacacia cl. Zhaiguan)*; Chinese Academy of Forestry: Beijing, China, 2007; pp. 12–14.
48. Persson, H. Root dynamics in a Young Scots pine stand in central Sweden. *Oikos* **1978**, *30*, 508–519. [CrossRef]
49. Ciren, Q.X. *The Study of Rainfall Redistribution and throughfall Spatial Heterogeneity of Artificial Pinus tabulaeformis Forest in Loess Region of Western Shanxi Province*; Beijing Forestry University: Beijing, China; 2014; Volume 20.
50. Pan, D.; Bi, H.X.; Ciren, Q.X.; Wang, L.L.; Gao, L.B.; Xu, H.S.; Bao, B. Relationship between environmental factors and water consumption regularity of typical forest vegetation in loess region of western Shanxi Province, northern China. *J. Beijing For. Univ.* **2013**, *35*, 17. [CrossRef]
51. Hsiao, T.C. Plant responses to water stress. *Annu. Rev. Plant Physiol.* **1973**, *24*, 519–570. [CrossRef]
52. Jamaludheen, V.; Kmumar, B.M.; Wahid, P.A.; Kamalam, N.V. Root distribution pattern of the wild jack tree as studied by 32 P soil injection method. *Agrofor. Syst.* **1996**, *35*, 329–336. [CrossRef]
53. Wang, Z.Q.; Liu, B.Y.; Zhang, Y. Soil moisture of different vegetation types on the Loess Plateau. *J. Geogr. Sci.* **2009**, *19*, 710. [CrossRef]
54. Yang, L.; Wei, W.; Chen, L.D.; Cai, G.J.; Jia, F.Y. Soil desiccation in deep soil layers under different vegetation types in the semi-arid loess hilly region. *Geogr. Res.* **2012**, *31*, 71–81. [CrossRef]
55. Li, J.; Wang, X.C.; Shao, M.A.; Zhao, Y.J.; Li, X.F. Simulation of water-limiting biomass productivity of Chinese Pine plantations and the soil desiccation effect in 3 Sites with different annual precipitation on Loess Plateau. *Sci. Silva. Sin.* **2010**, *46*, 33. [CrossRef]

56. Niu, J.J.; Zhao, J.B. *Soil Water Environment and Vegetation Construction in Shanxi*, 1st ed.; China Environmental Press: Beijing, China, 2008; pp. 66–67. ISBN:9787802097575.
57. Rodriguez-Iturbe, I.; Porporato, A.; Laio, F.; Ridolfi, L. Plants in water-controlled ecosystems: Active role in hydrologic processes and response to water stress: I. Scope and general outline. *Adv. Water Resour.* **2001**, *24*, 698. [CrossRef]